Hindawi
Advances in Civil Engineering
Volume 2019, Article ID 9081586, 11 pages
https://doi.org/10.1155/2019/9081586

Research Article

Experimental Study on the Nonlinear Behavior of a Sailing Container Ship under Landslide-Induced Surges

Pei-yin Yuan,[1,2] **Ping-yi Wang**,[1] **Yu Zhao**,[1,3] **and Mei-li Wang**[1,3]

[1]*College of River and Ocean Engineering, Chongqing Jiaotong University, Chongqing 400074, China*
[2]*College of Shipping and Naval Architecture, Chongqing Jiaotong University, Chongqing 400074, China*
[3]*College of Architecture and Urban Planning, Chongqing Jiaotong University, Chongqing 400074, China*

Correspondence should be addressed to Pei-yin Yuan; yuan_pei_yin@163.com

Received 12 September 2018; Revised 9 December 2018; Accepted 8 January 2019; Published 3 February 2019

Academic Editor: Chiara Bedon

Surges induced by rock landslides that enter water at a high speed are extremely destructive. The initial surge height and spread characteristic are important references used in disaster precaution and risk assessment. In this study, twenty groups of orthogonal experiments of landslide-induced impulse wave were conducted, the details of the self-propulsion of ships were designed, the values of the propeller, rudder, and shafting were calculated, and the model of the propeller and rudder was processed. The validity of the model system was verified from a turning test, zig-zag maneuver test, and free attenuation test. The interactions between landslides and water and between landslide-induced wave and ships are analyzed by performing an orthogonal model test and determining the difference among the initial wave heights of landslide surges caused by different landslide volumes. The model test can compare and analyze the influences of different landslide volumes and navigation positions on the nonlinear behavior of ships, thereby proposing control methods and measures for safe sailing in waters with landslide-induced surges and providing a theoretical basis for disaster prevention and reduction in the channel of a reservoir area or a hydraulic structure.

1. Introduction

The height of waves can range from tens of meters to over 100 m when the water rushing to the opposite bank or to water-retaining structures is stirred up by large surges such as a large landslide body from the reservoir bank rushing into the reservoir at a high speed [1–3]. Simultaneously, the shape and depth of a river channel in a reservoir area are extremely complicated, and the time that a surge wave reaches the shore varies. Some surge waves will rise, whereas others will exhibit reflection and refraction, thereby generating extremely complex fluctuations on the water surface of the entire reservoir area [4, 5]. Landslide-induced surges may cross the dam crest and may destroy hydraulic buildings and threaten the safety of dams and downstream properties. Rocky soil from landslides may block rivers, particularly in severe cases [6]. Therefore, the effect of landslide-induced surge on ships should be taken into account.

In recent years, extensive analytical investigations have been performed to study the motions of extremely large ships during tsunami, and an effective floating tsunami protection wharf was established [7–9]. To investigate the motions of a tsunami, Makino and Koba [10] proposed a new method based on the big data of a vessel. The big data of a ship refer to a collective data group that consists of the data sent from the ship's journey and the details of the ship's journey. A number of numerical simulations investigated vessel motions and considered several feasible scenarios to evaluate the progress of appropriate discrete-event simulation-based ship evacuation processes [11, 12]. The time-domain Rankine source method was developed to solve

motion of ship advancing with steady forward speed in waves [13, 14]. The authors reviewed the progress of ship antiroll tanks and developed a quasi-linear theory for "rectangular" antirolling tanks [15, 16]. The motion characteristics of ships were studied with four degrees of freedom, and the near-field and far-field disturbances in Green's function by Faltinsen and Michelsen [17], Fein et al. [18] and Scullen and Tuck [19]. Sen [20] evaluated the effects of nonlinear terms on the calculation results of the motion response of a ship. Bulian and Cercos-Pita addressed ship dynamics in presence of sloshing, coupled with a 3D weakly compressible smoothed-particle hydrodynamics [21]. Wu and Hermundstad [22] used nonlinear time-domain equations to calculate ship motion response and wave load. Aniel-Quiroga et al. studied the interaction between tsunami waves and coastal structures as these are the first to receive the tsunami's energy [23]. The probability of invasion was lowered for the Gulf of Alaska and Hawaii [24, 25]. Silva and Soares [26] described a nonlinear strip theory model in the time domain of ship motions with six degrees of freedom. Neves and Rodríguez [27] introduced a third-order mathematical model to illustrate the intense parametric excitation related to cyclic changes in the restoration features of a vessel.

Recently, some experimental tests have been performed to investigate the characteristics of landslide-induced waves and ship motions. Ataie-Ashtiani and Nik-Khah [28] analyzed the wave period, amplitude, and energy caused by surges by conducting 120 sets of model tests. Fritz et al. [1] considered the effects of different characteristic parameters on surges through three-dimensional physical tests and analyzed the flow field characteristics caused by surges. de Carvalho and Antunes do Carmo [29] investigated the influencing factors and pressure magnitude on a reservoir bank of landslide-induced surges by conducting model tests. Some investigations have been performed based on basic theory. Sayed and Hamed [30] assessed the reaction of a two degree-of-freedom quadratic coupling system with the effects of parametric and harmonic excitations. Heller and Hager [5] analyzed the waveform characteristics of the pulse waves generated by landslide-induced surges based on nonlinear theory. A ship model resistance test was conducted to study the motion of the ship model in ice floes [31].

In the Three Gorges Reservoir, the volume of 24 million soil slid into the channel river, cut off the river, and caused a landslide-induced wave that is more than 20 m high that capsized some ships, thus causing significant economic losses. The interaction between a landslide-induced wave and a ship is seldom studied. This paper investigates the propagation law of landslide-induced surges in complex curved river channels, strengthens the early warning and prevention of geological disasters in reservoir areas, and explores the nonlinear effects of landslide-induced surges on the primary degree-of-freedom motion response of a ship based on a series of landslide surge tests. The safe navigation range of ships in the reservoir area is also evaluated.

2. Model Test Design

2.1. River Channel Model. This study is based on the situation of a river wharf section in the Three Gorges Reservoir. The river channel model adopts a geometric scale of 1 : 70 to simulate the river section, which is from the 36 km mileage to the 330 km mileage of the channel river, and the length is approximately 6 km. The model was constructed using a section method, and the river bottom terrain was produced. The generalized model can analyze the dynamic changes of a landslide body. The landslide body was built with a certain ratio that adopted a number of stones with different specifications according to survey data. The friction coefficient is reduced owing to the pressure reduction between stones and particles when fine particles slide between the stones. Figure 1 shows the topographic drawing of the channel. In the model test, the channel model was built according to the actual scale ratio, as shown in Figure 2.

2.2. Ship Model. According to the survey data, owing to the rapid development of the local economy, a container ship is the primary ship type around the region of landslides. Last year, the containerized freight volume was 1.152 million tons, and the trend is gradually increasing. Such an external environment imposes increasingly higher requirements on the tonnage of ships and the navigation capacity of waterways. The ship type is a 3500T container ship in the model test. The survey data are shown in Figure 3.

The ship model was designed at a scale of 1 : 70 based on geometric similarity, similar gravity, and similar motion. The ship model was self-navigating and made of wood boards, wooden strips, and fiber-reinforced plastic (FRP). The longitudinal and transverse skeletons of the ship were first produced following the design drawings of the ship. Subsequently, the outer and inner plates of the ship were cut, bent, and fixed by bonding. The ship was coated with glass FRP to waterproof it. Finally, the completed ship model was verified and painted. The data are shown in Table 1. These data include the primary dimensions of the container ship, revolutions per second, torque and thrust values, rudder dimensions, etc.

The motive power of a sailing ship depends on the motor, the motor was linked to the propeller by the shafting, rotational speed of propeller count on the value of different voltages. The primary parameters of the motor are shown in Table 2.

The design of the shafting was based on the design specifications of the ship, and the diameter of the shafting is not less than the calculated results, as follows:

$$d = 98K\sqrt[3]{\frac{N_e}{n_e}\left(\frac{570}{\sigma_b + 157}\right)}, \quad (1)$$

where d indicates the diameter of the shafting, K indicates a coefficient, $K = 1.26$, N_e indicates the power of the shafting, n_e indicates the speed of the shafting, and σ_b indicates the tensile strength of the material.

Figure 1: Topographic drawing of the channel.

Figure 2: Layout of channel model.

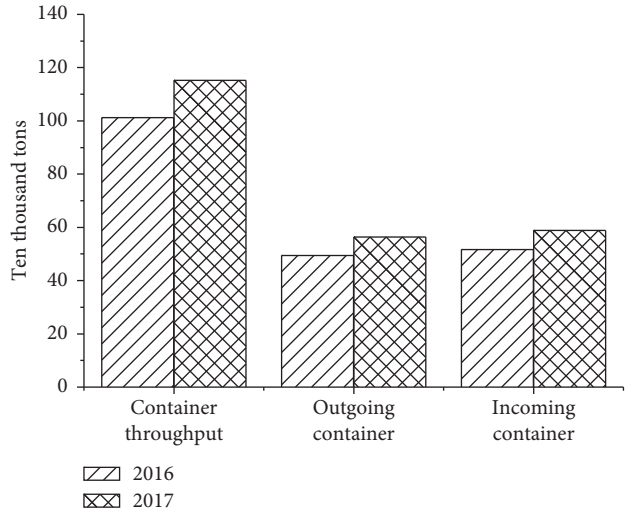

Figure 3: Bar chart of container throughput.

The design of the propeller should not only satisfy the requirements of installation, but should also satisfy the requirements of design speed. According to the parameters of the ship and the empirical formula, the specific parameters of the propeller are shown in Table 1, and the propeller geometry is shown in Figure 3.

The size of the rudder area will affect the maneuverability of the ship. If the rudder area is maintained within a reasonable range, the navigation resistance of the ship will not increase, and the navigation stability of the ship will be maintained. According to the empirical formula, the calculation is as follows:

$$\mu = 0.72 * \left(0.55 - 0.004 * \frac{L}{V}\right) * \frac{C_b * B}{L},$$
$$A_R = \mu L d\,(1 + 0.08). \tag{2}$$

According to the rules of shipbuilding, the total area of the rudder is not less than that calculated using the following formula:

$$A_R = \frac{TL}{100}\left[1 + 50C_b^2\left(\frac{B}{L}\right)^2\right]. \tag{3}$$

The specific parameters of the rudder are shown in Table 1. The rudder geometry is shown in Figure 4. Figure 4 shows the photograph of the ship model, propeller geometry, rudder geometry, and the details of the self-propulsion.

Table 1: Primary parameters of the ship.

Parameter	Real ship	Ship model
Length (m)	94.5	1.350
Beam (m)	15.1	0.216
Deep (m)	9.0	0.129
Draft (m)	5.6	0.08
Cb	0.7	0.7
Cp	0.69	0.69
Displacement (t/g)	3500 t	10150 g
Area of rudder (m^2/cm^2)	14.3	2.9
Rudder height (m/cm)	4.1	5.9
Aspect ratio	1.72	1.72
Number of blades Z	4	4
Propeller diameter (m/cm)	3.1	4.4
Screw pitch (m/cm)	2.6	3.7
Disk ratio	0.67	0.67

Table 2: Primary parameters of motor.

Voltage	Power	Maximum speed	Maximum torque	Reduction ratio
24 V	750 W	3000 r/min	4.6 Nm	2.23 : 1

2.3. Arrangement of Channel and Measuring Points. In accordance with the second point of Article 10, Chapter 2 of the Regulations on Navigation Safety of the Water Traffic Control Area of the Three Gorges Water Control Project (2016), a ship should rely on the channel on the starboard side when navigating the Three Gorges Reservoir. During the test, the ship model may exhibit a large amplitude sway under landslide surges, which causes yaw, collision, stranding, and other accidents. To ensure a successful test, the final route was set to 0.5 m from the right side of the centerline of the channel and 3.5 m from the shore.

Five experiments were performed for each group; the first experiment was to determine the position of the initial

Figure 4: Ship model.

impulse wave and to affix the wave gauges. The second experiment was to determine the position of the container ship and to improve the accuracy of the measurement. The others were to acquire the height of the initial wave and the motion values of the ship about the roll and pitch; subsequently, the average values of those data were calculated as the experimental values of the results of the group.

In the model test, monitoring point no. 2 is the intersection of the landslide track extension line and the navigation line. Monitoring point no. 3 is the intersection of the middle section of the curve and the navigation line. Monitoring point no. 1 is located on a straight segment. The distance from the first point to the second point is equal to the distance between the second and third points, as shown in Figure 5. The sliding blocks are according to the actual situation of the landslide and are composed of different sizes, as shown in Figure 6.

3. Test Conditions

The design of the rocky landslide model adopts a single-factor test for the plan. Considering that the horizontal velocity component of landslide body is larger, the energy exchange between the landslide and the water is sufficient. An angle of 40° was selected for the landslide to enter the water. The water has three levels: 145, 155, and 175 m, during the operation of the Three Gorges Reservoir. Combined with the actual water level during operation and the depth of the river, the river channel is generally processed for testing and other elements. The water level for the model test was set to 0.74 m based on the scale ratio conversion. The ship sails along the prefabricated route at a constant speed of 0.7 m/s and passes through position nos. 1, 2, and 3 to investigate the surges of two landslides with different volumes in the water and the influence of complex motions on the response of the ship. The first landslide has a length of 1 m, a width of 0.5 m, and a thickness of 0.6 m. The second landslide has a length of 1 m, a width of 1.5 m, and a thickness of 0.4 m. The water is still, and wind is absent during the test. The model test consists of 45 groups, and the typical conditions of the test for four groups are provided in Table 3.

4. Experimental Verification

4.1. Experimental Verification of Landslide-Induced Wave. In order to verify the correctness of the model test, this paper selects the same experimental model and test parameters as that of the Heinrich [32]. The landslide body size is 0.5 m ∗ 0.5 m. The angle of slope is 45 degrees, and the depth of water is 0.4 m. The landslide body slides under the action of gravity. The experimental results coincide with that of Heinrich basically. Therefore, this paper establishes the experimental model which can simulate landslide-induce wave accurately (Figure 7).

4.2. Turning Test. To verify the validity of the model test, the maneuverability of the ship is decided by the steering, turning, collision avoidance, and other behaviors, which are closely related to the ship's rotary performance. Therefore, the rotary performance of the ship is the only standard to measure the maneuverability of the ship. The rotary test was performed in the laboratory of Chongqing Jiaotong University. The experimental tank is 50 m long and 30 m wide. The rotary program was written using Visual Basic language, and a Differential Global Positioning System (DGPS) was equipped within the ship to capture its position information during navigation.

In order to obtain the higher accuracy of the position, the position system of DGPS and the differential technology were used in the process of the model test. A GPS receiver was placed on the reference station for observation. Based on the precise coordinates of the reference station, the corrected data from the reference station to satellite were calculated; the accurate data were sent out promptly, and the corrected data were observed and received by the reference station. The information of trajectory was corrected, thus improving the accuracy of the positioning.

At the beginning of the model test, the angle of the rudder was controlled zero, the ship was maintained in a straight line, and a signal was sent to change the rudder angle. Next, the ship model started to enter the rotational motion, and the position information was recorded by DGPS during the model test. When the ship entered a stable state of rotation, the diameter of rotation was recorded. The data of the turning test in the state of 15°, 25°, and 35° are shown in Figure 8. The results of turning test conformed to the basic requirements of ship model. The turning test results of different rudder angles are shown in Table 4.

4.3. Zig-Zag Maneuver Test. To verify the validity of the model test and to study the maneuvering state of the ship model in the water area, the zig-zag maneuver test was performed. The voltage of the primary engine of the ship was

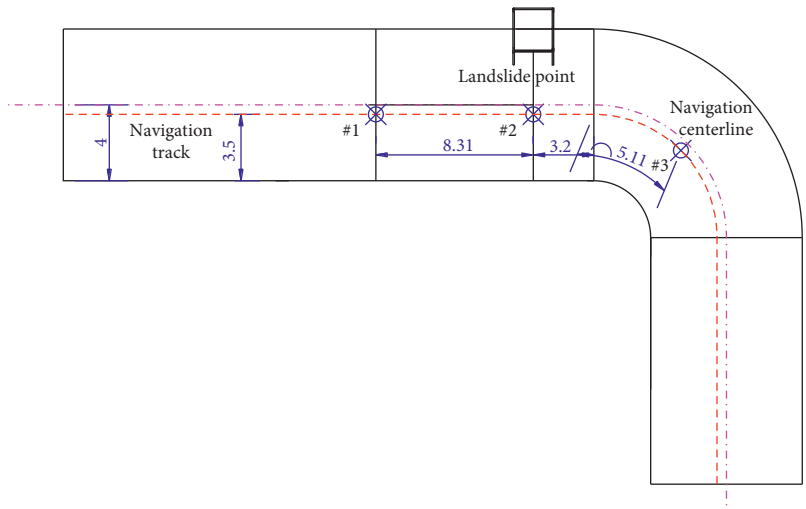

Figure 5: Route and layout of measuring points.

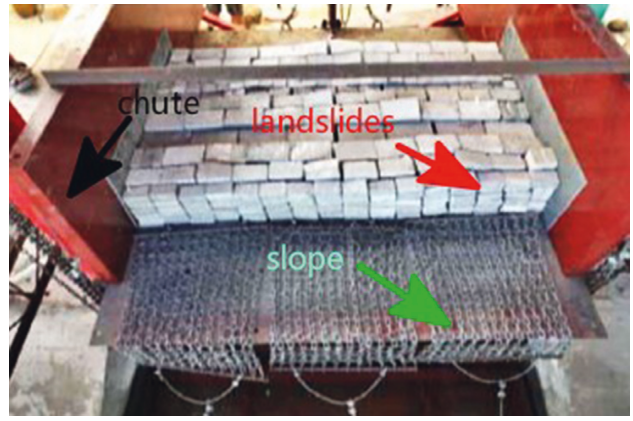

Figure 6: Arrangement of sliding blocks.

Table 3: Operating of the test.

Number	Angle of entering water (°)	Water depth (m)	Speed (m/s)	Position of ships	Landslide volume ($L \times B \times D$ (m))
Case 1	40	0.74	0.7	1	$1 \times 0.5 \times 0.6$
Case 2	40	0.74	0.7	2	$1 \times 0.5 \times 0.6$
Case 3	40	0.74	0.7	3	$1 \times 0.5 \times 0.6$
Case 4	40	0.74	0.7	2	$1 \times 1.5 \times 0.4$

controlled before the model test, and the ship was sailing in a straight line at a fixed speed. The steering command was issued by the controller. First, the ship model should steer 10° to the right and this state was maintained. Gradually, the ship model should turn to the right. When the heading angle is 10°, the ship model should steer 10° to the left and maintain this state. The ship model turned to the right and the angular velocity of the bow decreased gradually until it disappeared, and then the ship model turned to the left. When the bow angle is the same as the rudder angle, the rudder was turned to the right. The process above was recorded, and the navigation position and trajectory of the ship model were recorded by DGPS. The data of the zig-zag maneuver test in the state of 10° and 20° are shown in Figure 9. The results of the zig-zag maneuver test conformed to the basic requirements of ship model.

It can be seen from Figure 9 that the general trend of trajectory is consistent, the error is less than 10%, and the model test meets the requirements of accuracy, so it can provide the guarantee for the results of the model test. However, there is no symmetry with respect to y displacement value, and the main reasons are as follows:

Firstly, the model test was carried out in the pool of Chongqing Jiaotong University. As a result, it was difficult to achieve the ideal situation of no wind and no flow. Secondly, the actual loading condition of container ship was carried

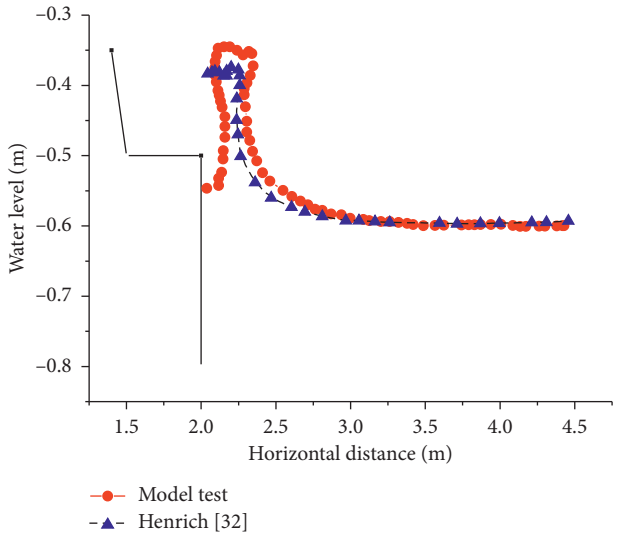

Figure 7: Comparison between Heinrich [32] and experimental free surface at 0.6 s.

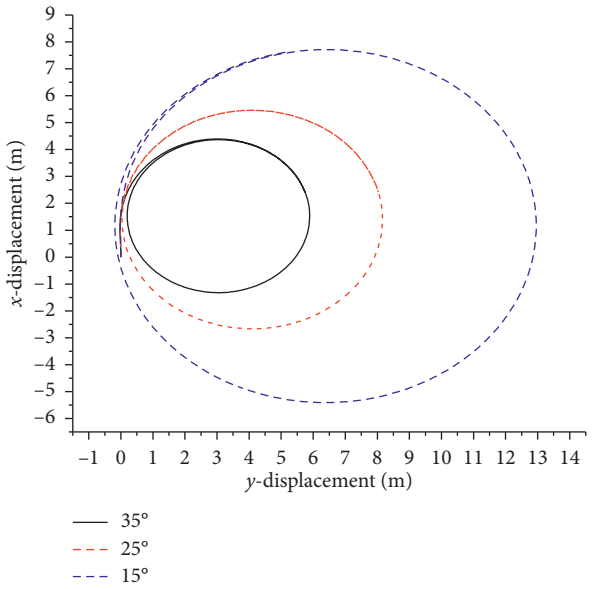

Figure 8: Trajectory in the turning test recorded by DGPS.

Table 4: Turning test data.

Element	Test results		
Rudder angle (°)	35	25	15
Speed of ship (m/s)		0.7	
Vertical intercept (m)	4.3	5.3	7.6
Horizontal intercept (m)	2.1	3.1	5.2
Turning radius (m)	5.7	8.1	13.1

out in the process of model test that was not up to fully loaded condition. Thirdly, the interaction between propeller and rudder affected the efficiency of the rudder. Lastly, the process of steering was linear; the actual situation was in inconsistent with it; the response of ship model to the rudder

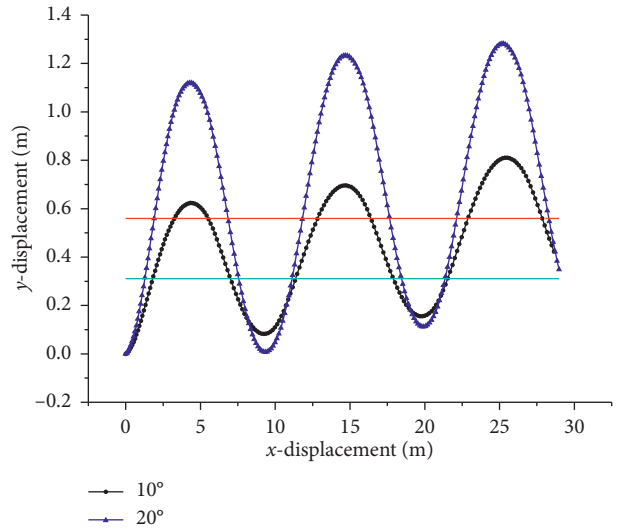

Figure 9: Trajectory in the zig-zag maneuver test recorded by DGPS.

deflection was very slow and so it becomes difficult to determine the suitable frequency of hydrodynamic forces.

As we can see from Figure 10, with the increase of rudder angle, the heading angle increases gradually, the differences between two cases are very small, and the time history curves of the heading angle and rudder angle agree well with the requirements of the standards for ship maneuverability resolution [33, 34]. It contains the 1st and 2nd overshoot angle. The response of ship to the first rudder angle is in good agreement with the first overshoot angle. This shows that ship model has better maneuverability.

4.4. Free Attenuation Test. The degrees of freedom of the motion of the ship in the vertical plane exhibit the recovery characteristic. The ship model deviates from the position of equilibrium under an external loading. When the external force disappears, the ship will return to the original position, which depends on its own recovery characteristic. Under the free state, the roll motion and pitch motion of the ship are attenuated in static water. The natural period and dimensionless damping coefficient can be obtained by analyzing the attenuation curve; subsequently, the accuracy of model test can be verified. The decay curve of roll motion is shown in Figure 11, and the decay curve of pitch motion is shown in Figure 12.

5. Analysis of Test Results

5.1. Propagation Characteristics of Landslide Surge. The wave height and landslide surge cycle were measured using an ultrasonic wave acquisition analyzer designed and developed by the Southwest Transportation Science Research Institute of Chongqing Jiaotong University. Seven measuring points, which measure the initial surge and the surge along the path, were established. The straight road, curve, and river section areas were the primary measurement areas. Among the measuring points, measuring point no. 1 is the center point

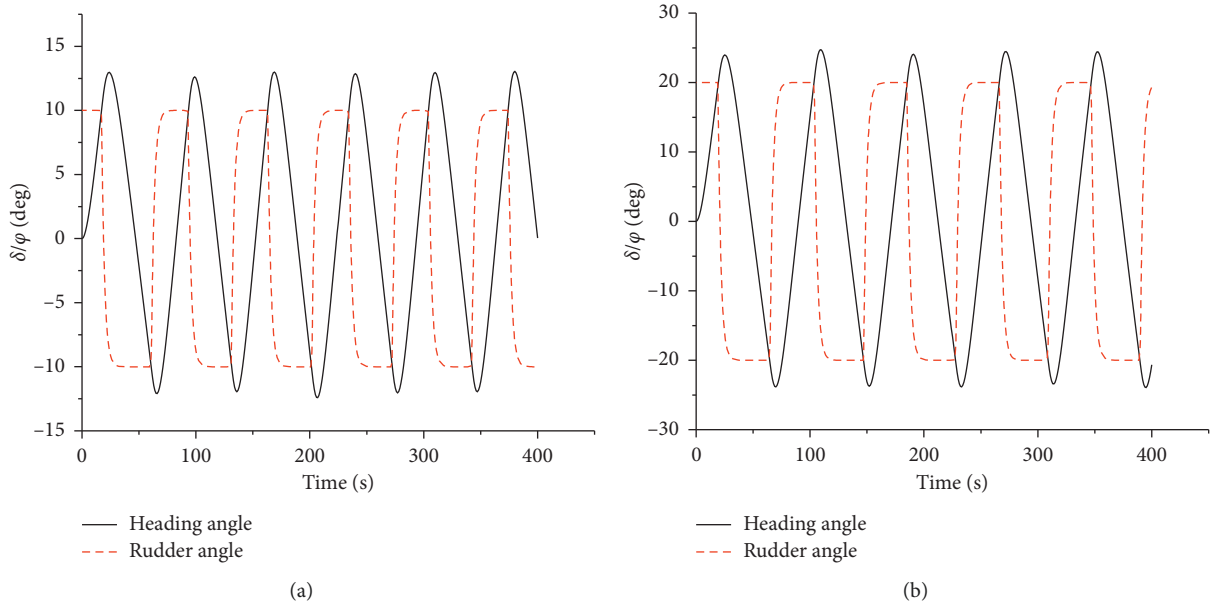

Figure 10: Results of zig-zag test. (a) Time history curve of heading angle 10. (b) Time history curve of heading angle 20.

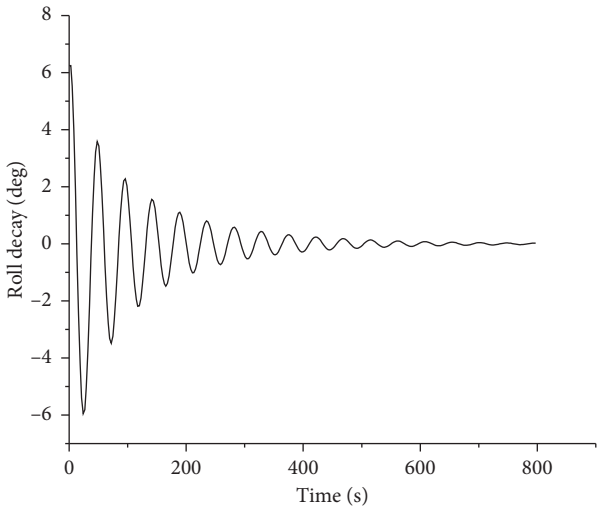

Figure 11: Decay curve of roll motion.

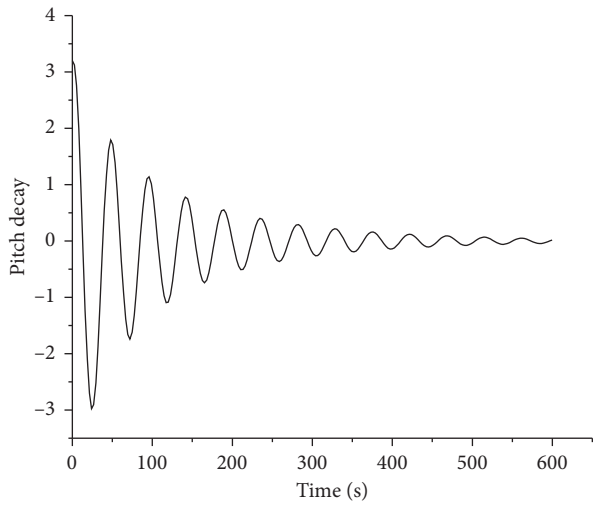

Figure 12: Decay curve of pitch motion.

of the area where the landslide enters the water. The data acquisition system collects the wave height and period data from different areas. The acquisition time is generally 200 s, and the frequency is 50 Hz. Two types of landslide bodies enter the water during the test. The large landslide volume has a length of 1 m, a width of 1.5 m, and a thickness of 0.4 m. The small landslide volume has a length of 1 m, a width of 0.5 m, and a thickness of 0.6 m.

Figure 13 shows that a certain delay occurs in the landslide data, under different volumes, with the same entrance angle into the channel model of 0.74 m. The landslide-induced surge is irregular and asymmetric under the two operating conditions. The surges are spread incompletely during the early stage of landslide entry into the water. Over time, the front edge of the surges becomes steep and the water level rises and reaches its maximum value within an extremely short time. The wave height decreases rapidly and becomes a small-amplitude oscillation, and the water surface gradually returns to the stationary state after the landslide surge reaches a high peak. The landslides with different volumes are accompanied by considerable energy loss as they enter the water. The lost energy is transformed into the heat energy and kinetic energy of the water. The height of the first wave caused by the landslide is different. The volume of the large landslide is twice that of the small landslide. The height of the first wave generated by the large landslide is thrice that of the small landslide. The height of the first wave caused by the landslide body that entered the water increases with landslide volume. When the landslide that enters the water has a different volume, the time that the first wave

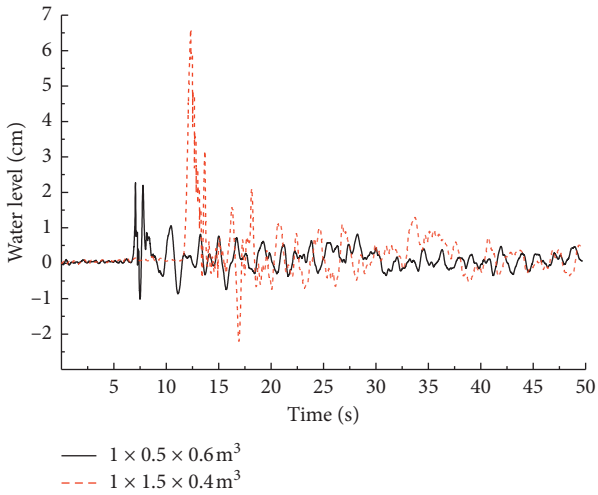

Figure 13: Height of the first wave caused by landslides with different square volumes. The labels are length, width, and thickness in sequence, such as the length is 1 m, the width is 0.5 m, the thickness is 0.6 m.

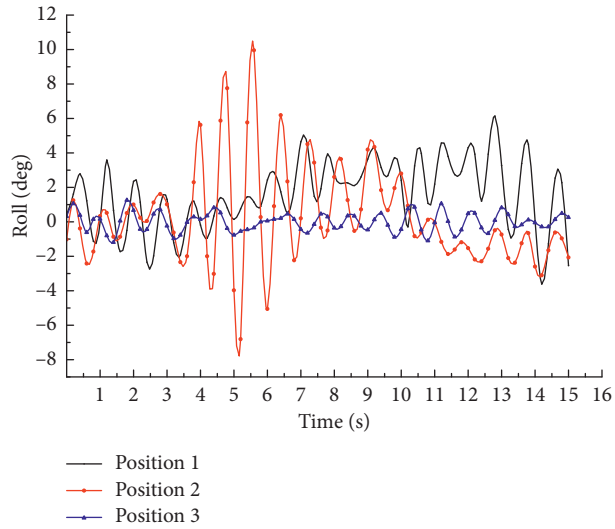

Figure 14: Time history curve of the rolling motion of the ship under different navigational positions.

height reaches its peak varies. When the landslide volume is large and the speed of the spreading surges caused by the landslide entering the water is fast, the water waves spreading along the coast and the influential scope of the disaster are expanded.

5.2. Influence of Different Navigation Positions on Ship Motion Response. The rectangular landslide block enters the water with a length of 1 m, a width of 0.5 m, and a thickness of 0.6 m when the ship passes the river's monitoring points 1, 2, and 3 at a constant speed of 0.7 m/s. The self-developed ship attitude acquisition device measures the rolling motion and pitch motion amplitudes of the ship and subsequently compares and analyzes the relevant provisions of the Inland River Ships Statutory Inspection Technical Regulations to determine the safe navigation range of the ship.

As shown in Figure 14, the shapes of the rolling motion curve at three locations are similar and a time difference of the maximum peak period node exists. The ship model sailed to different positions, and the maximum amplitude of the rolling motion satisfied the requirements of the rules. The landslide-induced surges carried most of the energy to the vicinity of the ship and generated the maximum hydrodynamic pressure on the ship. The landslide body enters the water when the ship sails to position no. 1. The landslide surge is centered on the entry point of the landslide body, scatters and propagates around it, and interacts with the ship. The ship has a rolling motion amplitude of 4°, and it continues to sail forward. The ship acquires a large rolling motion amplitude after encountering the secondary wave of the landslide surge and the reflected wave on the opposite bank, with a maximum value of 6°. The ship depends on its own recovery torque and recovery damping and gradually returns to a stable state. The landslide surge occurs suddenly when the ship sails to position no. 2, and the ship has a large rolling motion amplitude with a maximum value of 11°. Moreover, the motion amplitude of the ship is gradually reduced when the ship encounters an initial high peak surge. The landslide body enters the water at a high speed when the ship travels to position no. 3. A chasing state occurs between the landslide-induced surge and the sailing ship. Energy decreases gradually with an increase in the propagation distance of the wave surges, which has a minimal effect on the ship's rolling motion amplitude. The rolling motion amplitude of the ship exhibits a small fluctuation and is relatively stable.

As shown in Figure 15, a landslide occurs when the ship sails to position nos. 1, 2, and 3. The ship model sailed to those different positions, and the maximum amplitude of the pitching motion satisfied the requirements of the rules. The maximum rolling direction of position nos. 1 and 2 is different and noticeable and is attributed to the difference in the force position of the ship depending on the landslide surge. The landslide surge acts on the stern of the ship when the ship sails at position no. 1, and the maximum pitch value is 1.8°. The landslide surge acts on the tail of the ship when the ship sails at position no. 2, and the maximum pitch value is 1.25°. The speed of the landslide surge is less than that of the ship when the ship sails to position no. 3. The ship sails in still water to generate waves caused by its traveling. After the reflection onto the bank wall, a small amplitude effect is observed on the ship's pitch.

5.3. Influence of Different Quantities of Landslides on Ship's Motion Response. Figure 16 shows the effect of different numbers of landslides on the ship's motion response after the landslides enter the water. The maximum amplitude of the rolling motion of the ship model satisfied the requirements of the rules. The landslide-induced surge spreads into the channel and interacts with the ship after a large number of landslide bodies (length = 1 m, width = 1.5 m, and height = 0.4 m) enter the water. The waveforms differ slightly

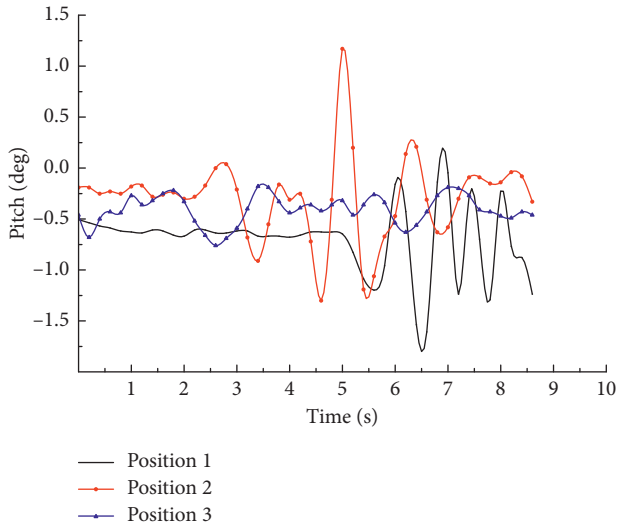

Figure 15: Time history curve of the pitching motion of the ship under different navigation positions.

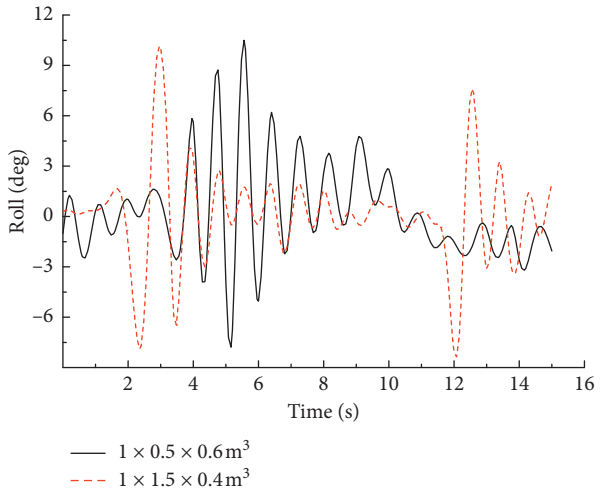

Figure 16: Time history curve of the rolling motion of the ship with different numbers of landslides. The labels are length, width, and thickness in sequence, such as the length is 1 m, the width is 0.5 m, and the thickness is 0.6 m.

when the surges caused by different numbers of landslides are transmitted to the vicinity of the ship.

The time history curve of the ship's rolling motion contains two peaks. The first peak is reached when the initial surge propagates to the ship's navigation position and interacts with the ship. The maximum amplitude of the rolling motion is 10.5°, and the reverse effect of the landslide surge is not initiated. The second peak occurs when the landslide-induced surge impacts the soil bank slope. The water depth becomes shallow and narrow, the wave energy gathers, and the surge wave spreads slowly. At this point, a wave propagates at a slightly slower speed, and its latter peak cannot catch up. A certain degree of water wall is formed after the reflection across the opposite shore, which interacts with the ship. The maximum rolling motion amplitude is 8.5°, and the ship's rolling amplitude decreases with time. The secondary damage of the ship caused by the landslide-induced surge and the violent shaking degree of the ship under the landslide-induced surge should be considered during a real voyage. The shifting of the ship's load, which changes the overall center of gravity of the ship and causes it to tilt, should be prevented. The stability of the ship increasingly deteriorates, and the ship's recovery torque becomes smaller than the external moment of the landslide, thereby causing the ship to overturn.

As shown in Figure 17, the ship experiences landslide surges caused by different landslide bodies that enter the water during its voyage. The maximum amplitude of the pitching motion of the ship model satisfied the requirements of the rules. The change in the ship's pitch undergoes occurrence, development, and decay processes with remarkable changes in the pitching motion amplitude of the ship. The propagation speed of the landslide surges is relatively fast, the interaction with the ship is early, and the maximum longitudinal amplitude is 1.75° when a large number of landslide bodies enter the water. The interaction time with the ship is delayed, and the maximum longitudinal amplitude is 1.25° when a small number of landslide bodies enter the water. The effect of landslide surges caused by different numbers of landslides on the ship's pitching motion exhibits a single-peak effect. The impact of the initial surge on the ship should be considered during the ship's navigation. The ship stall caused by a huge landslide surge, which deviates from the channel, pushes the ship toward the shore, and causes the ship to overturn and sink, should be investigated.

The primary engine should be started, the bow direction should be adjusted appropriately, and the spread direction of the landslide-induced surge should be forwarded when a sudden landslide occurs during the voyage. The minimum cross section of the bow should be swayed toward the landslide-induced surges to divert their direction from the two sides of the hull. The hull's own streamline can effectively disperse the impact of landslide-induced surges, thereby maximizing the ship's protection and is conducive to preventing the tilting or tipping over of the ship on one side owing to landslide-induced surges.

6. Discussion and Conclusions

Based on field investigations, literature review, and model tests, this study obtained the characteristics of a ship when landslide-induced surges occur, and the impact of these surges on the ship's motion response. The emergency situation of maintaining safe navigation when a landslide entered the water was assumed, which was conducive to engineering feasibility demonstration and governance. The conclusions are summarized as follows:

(1) The waveform of the landslide-induced surge exhibited evident asymmetry, wherein the peak was large and the trough was small with strong nonlinearity. The height of the wave decreased rapidly after the first wave of landslide-induced surge, and the wave energy decreased gradually with increased propagation distance.

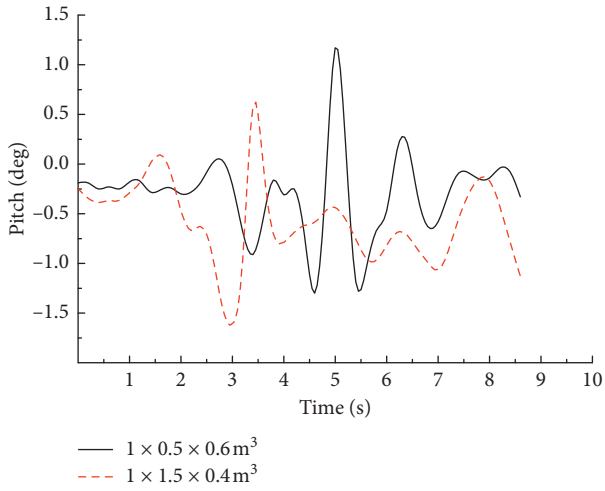

Figure 17: Time history curve of the pitching motion of the ship under different numbers of landslides. The labels are length, width and thickness in sequence, such as the length is 1 m, the width is 0.5 m, and the thickness is 0.6 m.

(2) The aspect ratio reduced when the volume of the landslide body was large, and the first wave height of the landslide-induced surge was high. When the number of landslides was large, the speed of landslide-induced surges was high.

(3) The landslide-induced surge exerted the greatest impact on the ship when it passed position no. 2, followed by position no. 1, and finally, position no. 3. In an actual navigation, the distance from the landslide point should be controlled, the impact of landslide-induced surges on the ship should be reduced, and the collision of the ship with coastal fixed structures and different degrees of damage under landslide-induced surges should be prevented.

(4) When the number of landslides was large, the impact on the motion response of a sailing ship was considerable. In engineering practice, the landslide volume should be controlled to prevent the impact of the first wave and secondary wave peaks on the ship. The secondary damage of landslide-induced surges to the ship should be considered, and a warning system for landslide-induced surge disasters should be constructed to reduce the damage to ships.

(5) A ship should be stagnated appropriately, the double anchors should be dropped, and the long anchor chain should be loosened to ensure the ship's stability, decrease the extent of rolling and pitch motions of the ship, and mitigate the impact of landslide-induced surges on the ship when large-scale landslide-induced surges occur during a voyage. The ship should wait for the gradual return of tranquility on the river surface and avoid dangerous water areas.

Data Availability

The figures and tables date used to support the findings of this study are included herein.

Conflicts of Interest

The authors declare that they have no conflicts of interest.

Acknowledgments

This study was supported by the National Natural Science Foundation (51479015) and Social Science and Technology Innovation Program for People's Livelihood in Chongqing (CSTC 2018jscx-msybx0233, cstc2017shms-zdyfX0026, and cstc2018jszx-cyzdX0019).

References

[1] H. M. Fritz, W. H. Hager, and H.-E. Minor, "Landslide generated impulse waves," *Experiments in Fluids*, vol. 35, no. 6, pp. 505–519, 2003.

[2] M. Quecedo, M. Pastor, and M. I. Herreros, "Numerical modelling of impulse wave generated by fast landslides," *International Journal for Numerical Methods in Engineering*, vol. 59, no. 12, pp. 1633–1656, 2004.

[3] H. Fuchs, V. Heller, and W. H. Hager, "Impulse wave run-over: experimental benchmark study for numerical modelling," *Experiments in Fluids*, vol. 49, no. 5, pp. 985–1004, 2010.

[4] V. Heller, W. H. Hager, and H.-E. Minor, "Scale effects in subaerial landslide generated impulse waves," *Experiments in Fluids*, vol. 44, no. 5, pp. 691–703, 2007.

[5] V. Heller and W. H. Hager, "Wave types of landslide generated impulse waves," *Ocean Engineering*, vol. 38, no. 4, pp. 630–640, 2011.

[6] K. Yin, "Physical model experiments of landslide-induced surge in Three Gorges Reservoir," *Earth Science*, vol. 37, no. 5, pp. 1067–1074, 2012.

[7] S. Sakakibara, I. Abe, M. Tsugane, and M. Kubo, "A study on emergency ship handling against tsunami for moored vessel in harbor basin by intentional ship grounding," *Journal of Japan Institute of Navigation*, vol. 128, pp. 251–260, 2013.

[8] K. Masuda, "On optimal method of mooring ship in floating tsunami protection wharf," in *Proceedings of ASME 2015 34th International Conference on Ocean, Offshore and Arctic Engineering (OMAE2015)*, St. John's, NL, Canada, May-June 2015.

[9] S. Shiotani, X. Liu, and C. Chen, "Investigation on the effects of a sailing ship motion by Tsunami," in *Proceedings of OCEANS 2015*, pp. 1–5, Genova, Italy, May 2015.

[10] H. Makino and T. Koba, "Research on understanding of tsunami movement using ship big data," *Journal of Japan Society of Civil Engineers, Ser. B2 (Coastal Engineering)*, vol. 70, no. 2, pp. 1421–1425, 2014.

[11] I.-S. Cho, "A study on dynamic analysis of moored ship motions by tsunami," *Journal of Korean Navigation and Port Research*, vol. 29, no. 8, pp. 661–666, 2005.

[12] T. Pitana and E. Kobayashi, "Optimization of ship evacuation procedures as part of tsunami preparation," *Journal of Simulation*, vol. 3, no. 4, pp. 235–247, 2017.

[13] X. Chen, R.-C. Zhu, W.-J. Zhou, and J. Zhao, "A 3D multi-domain high order boundary element method to evaluate time domain motions and added resistance of ship in waves," *Ocean Engineering*, vol. 159, pp. 112–128, 2018.

[14] X. Chen, R.-C. Zhu, J. Zhao, W.-J. Zhou, and J. Fan, "Study on weakly nonlinear motions of ship advancing in waves and influences of steady ship wave," *Ocean Engineering*, vol. 150, pp. 243–257, 2018.

[15] R. Moaleji and A. R. Greig, "On the development of ship anti-roll tanks," *Ocean Engineering*, vol. 34, no. 1, pp. 103–121, 2007.
[16] J. F. Dalzell, C. Wen-Hwa, and J. E. Modisette, "Studies of Ship Roll Stabilization Tanks," Defense Technical Information Center, Fort Belvoir, VA, USA, 1964.
[17] O. M. Faltinsen and F. C. Michelsen, "Motion of large structure in wave at zero Froude number," in *The Dynamics of Marine Vehicles and Structures in Wave*, R. E. D. Bishop and W. G. Price, Eds., Mechanical Engineering Publication Limited, New York, NY, USA, 1975.
[18] J. A. Fein, A. H. Magnuson, and D. D. Moran, "Dynamic performance of an air cushion vehicle in a marine environment," AIAA Paper 74-323, AIAA, Washington, DC, USA, 1978.
[19] D. C. Scullen and E. O. Tuck, *Sea Wave Pattern Evaluation—Pressure Distributions: Mathematical Formulation*, Scullen and Tuck Pty Ltd., Adelaide, Australia, 2001.
[20] D. Sen, "Time-domain computation of large amplitude 3D ship motions with forward speed," *Ocean Engineering*, vol. 29, no. 8, pp. 973–1002, 2009.
[21] G. Bulian and J. L. Cercos-Pita, "Co-simulation of ship motions and sloshing in tanks," *Ocean Engineering*, vol. 152, pp. 353–376, 2018.
[22] M. Wu and O. A. Hermundstad, "Time-domain simulation of wave-induced nonlinear motions and loads and its applications in ship design," *Marine Structures*, vol. 15, no. 6, pp. 561–597, 2002.
[23] Í. Aniel-Quiroga, C. Vidal, J. L. Lara, M. González, and Á. Sainz, "Stability of rubble-mound breakwaters under tsunami first impact and overflow based on laboratory experiments," *Coastal Engineering*, vol. 135, pp. 39–54, 2018.
[24] T. W. Therriault, J. C. Nelson, J. T. Carlton et al., "The invasion risk of species associated with Japanese Tsunami marine debris in pacific north America and Hawaii," *Marine Pollution Bulletin*, vol. 132, pp. 82–89, 2018.
[25] N. Maximenko, J. Hafner, M. Kamachi, and A. MacFadyen, "Numerical simulations of debris drift from the Great Japan Tsunami of 2011 and their verification with observational reports," *Marine Pollution Bulletin*, vol. 132, pp. 5–25, 2018.
[26] S. R. E. Silva and C. G. Soares, "Prediction of parametric rolling in waves with a time domain non-linear strip theory model," *Ocean Engineering*, vol. 72, no. 4, pp. 453–469, 2013.
[27] M. A. S. Neves and C. A. Rodríguez, "On unstable ship motions resulting from strong non-linear coupling," *Ocean Engineering*, vol. 33, no. 14-15, pp. 1853–1883, 2006.
[28] B. Ataie-Ashtiani and A. Nik-Khah, "Impulsive waves caused by subaerial landslides," *Environmental Fluid Mechanics*, vol. 8, no. 3, pp. 263–280, 2008.
[29] R. F. de Carvalho and J. S. Antunes do Carmo, "Landslides into reservoirs and their impacts on banks," *Environmental Fluid Mechanics*, vol. 7, no. 6, pp. 481–493, 2007.
[30] M. Sayed and Y. S. Hamed, "Stability and response of a nonlinear coupled pitch-roll ship model under parametric and harmonic excitations," *Nonlinear Dynamics*, vol. 64, no. 3, pp. 207–220, 2010.
[31] W.-Z. Luo, C.-Y. Guo, T.-C. Wu, and Y.-M. Su, "Experimental research on resistance and motion attitude variation of ship-wave-ice interaction in marginal ice zones," *Marine Structures*, vol. 58, pp. 399–415, 2018.
[32] P. Heinrich, "Nonlinear water waves generated by submarine and aerial landslides," *Journal of Waterway, Port, Coastal and Ocean, Engineering*, vol. 118, no. 3, pp. 223–238, 1992.
[33] International Maritime Organization (IMO), "Standards for ship maneuverability," Resolution MSC. 137(76), IMO, London, UK, 2002.
[34] International Maritime Organization (IMO), "Standards for ship maneuverability," Resolution MSC/Circ. 1053, IMO, London, UK, 2002.